CHAPTER IV
CHITOSAN-MAGNETITE NANOPARTICLES VIA "CLICK" CHEMISTRY

4.1 Abstract

Chitosan-magnetite nanoparticles by conjugating alkyne chitosan with azide magnetite nanoparticles via silane coupling agent under "click" chemistry is proposed. The functionalization of chitosan with propargyl bromide gives alkyne chitosan and the surface modification magnetite nanoparticles gives azide silane followed by the conjugation between two favors the "click" chemistry resulting in the formation of triazole linkage.

Keywords: "Click" chemistry, Magnetite nanoparticles, Chitosan

4.2 Introduction

Nowadays, magnetite nanoparticles are widely used in medical and pharmaceutical applications such as hyperthermia therapy (Kawai *et al.*, 2008), magnetic resonance image (MRI) (Berry *et al.*, 2003; Neuberger *et al.*, 2005), and biomolecule separation (Šafařík *et al.*, 2004) due to their biocompatible, non-toxic and superparamagnetic properties. However, the magnetite nanoparticles tend to form aggregation in media because of their high surface energy. This point has to be considered because the magnetic properties, dispersability, and cell penetration will decrease. Therefore, these nanoparticles have to be coated with other molecules to retain their properties for example, sodium oleate and polyethylene glycol (Sun *et al.*, 2006), silane (Randy *et al.*, 2007) and polymers such as *N*-carboxyethylchitosan and poly(2-acrylamido-2-methylpropanesulfonic acid) (Mincheva *et al.*, 2008). In addition, magnetic nanoparticles for biomaterials are another important point to be considered.

It is known that chitosan is widely applied for pharmaceutical and medical fields because it has biological (biocompatibility, biodegradability, low toxicity,

haemostatic, anticancerogen, and anticholestermic) and chemical (active amino, and hydroxyl groups) properties. In the past, chitosan coated on magnetite nanoparticles via physisorption such as electrostatic, hydrophilic or hydrophobic-van der Waals interaction, and via covalent bonds such as amide linkage (Yuan *et al.*, 2008; Alejandro *et al.*, 2009) were reported.

Considering specific molecular design, it is known that "click" chemistry is an approach to obtain triazole linkage which provides hydrogen bond and/or metal coordination networks and these networks are frequently involved with biosystem (Schilling C. *et al.*, 2009). Therefore, chitosan conjugated with magnetite nanoparticles via triazole group is another possible structure for biomaterial chitosan magnetite.

The present work, therefore, proposes a molecular design for chitosan-magnetite nanoparticles through silane coupling agent based on "click" chemistry. Chitosan is considered as an organic species to be modified to present alkyne groups. Silane coupling agent is applied for magnetite nanoparticles modification with azide groups. A simple conjugation between both species leads to 1, 2, 3-triazole linkage as a consequent of "click" chemistry.

4.3 Experimental Section

4.3.1 Materials

Acetic acid was purchased from Univar, Australia. Ammonium hydroxide (NH_4OH), dimethylformamide (DMF), dimethylsulfoxide-d_6 (DMSO-d_6), ferric chloride hexahydrate ($FeCl_3 \cdot 6H_2O$), ferrous chloride tetrahydrate ($FeCl_2 \cdot 4H_2O$), potassium carbonate (K_2CO_3), and triethylamine were bought from Merck, Germany. Low molecular weight chitosan (LCS, Mw=15000 g/mol, 90% degree of deacetylation) was a gift from Chitin Research Center, Chulalongkorn University, Thailand. (3-Chloropropyl)-trimethoxysilane, oleic acid, phthalic anhydride, and sodium hydride (NaH) were purchased from Sigma-Aldrich, Inc., USA. Sodium azide (NaN_3) and hydrazine were bought from Fluka Chemika, Switzerland. Propargyl bromide was purchased from Tokyo Kasei Kogyo Co., Ltd., Japan. Sodium hydroxide (NaOH) and potassium hydroxide (KOH) were perchased from

Carlo Erba, Italy. Acetone, dichloroethane, ethanol, hexane, tetrahydrofuran, and toluene were bought from RCI Labscan, Thailand. All of chemicals were used as obtained without further purification.

4.3.2 Instruments and Equipment

Structural analysis were carried out by using an Equinox 5 Bruker Fourier transform infrared spectrometer (FTIR) based on KBr and ZnSe methods, and an Avance 500 Bruker Biospin Nuclear magnetite spectroscope (NMR). The phase of iron oxide was recorded by a D/DMAX 2200 Rigaku wide angle X-ray diffractometer (WAXD) based on 5-90° 2Θ with a scanning rate of 2.5° 2Θ /min under 0.05° 2Θ/scan. Thermal properties of product were analyzed on a Perkin Elmer Pyris Diamond thermogravimetric/ differential thermal analyzer (TG/DTA) with a N_2 flow and a heating rate of 10 °C/min in range of 80-950°C. Hydrodynamic radius and zeta potential of the products in various pH and solvent conditions were identified on a Malvern Zeta Sizer Nano Series with a detection angle of 173°, dynamic light scattering (DLS). Dispersability image and individual size were recorded on a 100 kV H-7650 Hitachi transmission electron microscope (TEM) by using copper grid and carbon grid. Magnetismof the particles were evaluated by vibrating sample magnetometer (VSM) at Khonkaen University. Absorption of plasmid DNA (pDNA) colloidal solution of *E.coli* was elucidated by a UV-vis spectrophotometer at Mahidol University.

4.3.3 Synthesis of Alkyne-phthaloylchitosan

LCS was reacted with phthalic anhydride (5 mol equivalent to pyranose ring) in DMF for 6 hours at 120°C under vacuum and continuously stirred at 60°C under nitrogen atmosphere overnight (Yoksan *et al.*, 2003) (Figure 3.3 (a)). The cleare solution obtained was precipitated in cold water, washed in DI water, dialyzed for 5 days, and dried with freeze dry to obtain yellow powder product of phthaloylchitosan.

The phthaloylchitosan obtained was reacted with an excess propargyl bromide and a small amount of triethylamine at room temperature. Similarly, the reaction was carried out at 60, 90, and 120°C. The reaction was also carried out with a small amount of KOH, NaOH, and NaH as a catalyst at 60, 90, and 120°C, except

NaH at 0°C. The solution was precipitated in cold water, dialyzed for 5 days, and freeze dried to obtain yellowish powder of alkyne-phthaloylchitosan, **1**.

4.3.4 Synthesis of Azide-magnetite Nanoparticles

Magnetite was coated with oleic acid as reported by Liu *et al.*, 2010. Briefly, $FeCl_3 \cdot 6H_2O$ and $FeCl_2 \cdot 4H_2O$ were dissolved in DI water in the ratio of 2:1 under nitrogen atmosphere, followed by adding a small amount of oleic acid into the solution under stirring. After 30 mins stirring, a 25% NH_4OH solution was added dropwise within 15 mins to the mixture. The suspension was heated at 85°C for 1 h and the temperature was reduced to room temperature. Superfluous ammonium oleate in the black ferro-fluid was removed by dialyzing against DI water before freeze drying to obtain black particles of oleic-magnetite.

The as-synthesized oleic-magnetite nanoparticles were reacted with an excess amount of (3-chloropropyl)-trimethoxysilane containing a small amount of acetic acid as a catalyst at 60°C for 72 h. The particles were washed with tetrahydrofuran and acetone. In each step the particles were separated by a high power magnet. The particles were dried under vacuum at room temperature. In this step, the co-precipitation of $FeCl_3 \cdot 6H_2O$ and $FeCl_2 \cdot 4H_2O$ reaction was also carried out without oleic acid as a comparative study.

The as-synthesized chloro-magnetite nanoparticles were reacted with an excess amount of NaN_3 in DMF at 80°C for 72 h obtaining azide-magnetite nanoparticles, **2**. The nanoparticles were washed with DMF, ethanol, and acetone and dried under vacuum at room temperature. In this step, the reactions in hexane, toluene, and dichloroethane were also carried out as comparative studies.

4.3.5 Conjugation of Magnetite Nanoparticles with Chitosan via "click" Reaction

Azide magnetite nanoparticles were reacted with alkyne phthoylchitosan in DMF at room temperature for 72 h to obtain phthaloylchitosan-magnetite, **3**. In similar, the reactions at 50, 70, and 90°C were also carried out. The product obtained was separated by a high power magnet, and washed with DMF, toluene, and acetone many times. The powder was dried under high vacuum at room temperature.

The as-synthesized phthaloylchitosan-magnetite nanoparticles were deprotected phthalamido group reacting with excess hydrazine solution at 80°C overnight to obtain chitosan-magnetite, **4**. The chitosan-magnetite obtained was purified by a high power magnet, followed by washing with ethanol and acetone several times, and drying under high vacuum at room temperature.

4.3.6 Direct Conjugation of Chitosan and Magnetite Nanoparticles

Magnetite nanoparticles obtained from the co-precipitation of $Fe_2Cl_4 \cdot 4H_2O$ and $Fe_3Cl_6 \cdot 6H_2O$ in the ratio of 1:2 in 25% NH_4OH was coated with LCS (0.5 wt%) adding 2% acetic acid solution with vigorous stirring and ultrasonication for 20 min. Twenty-five percent of NH_4OH was added to the mixture. The product obtained was washed with water and vacuum dried.

4.3.7 DNA Separation Study

The *E. coli* in TE buffer solution was quantitatively analyzed based on absorptions at 260 and 280 nm^{-1} observed by UV-vis spectrometer. The chitosan-magnetite (0.5 mg) was added in the solution of *E. coli*, followed by incubating for 5 mins. The supernatant was collected and the UV absorption at 260 and 280 nm^{-1} were traced. In this step, other samples such as chitosan-magnetite via direct synthesis and Dynabeads® were also studied.

4.4 Results and discussions

4.4.1 Structural Characterization

Low molecular weight chitosan with degree of deacetylation characterized by ^1H NMR spectroscopy was 90%. In this work, chitosan-magnetite nanoparticles are designed based on coupling of alkyne phthaloylchitosan and azide magnetite Cu(I) free-"click" chemistry as shown in Scheme 4.1.

Scheme 4.1

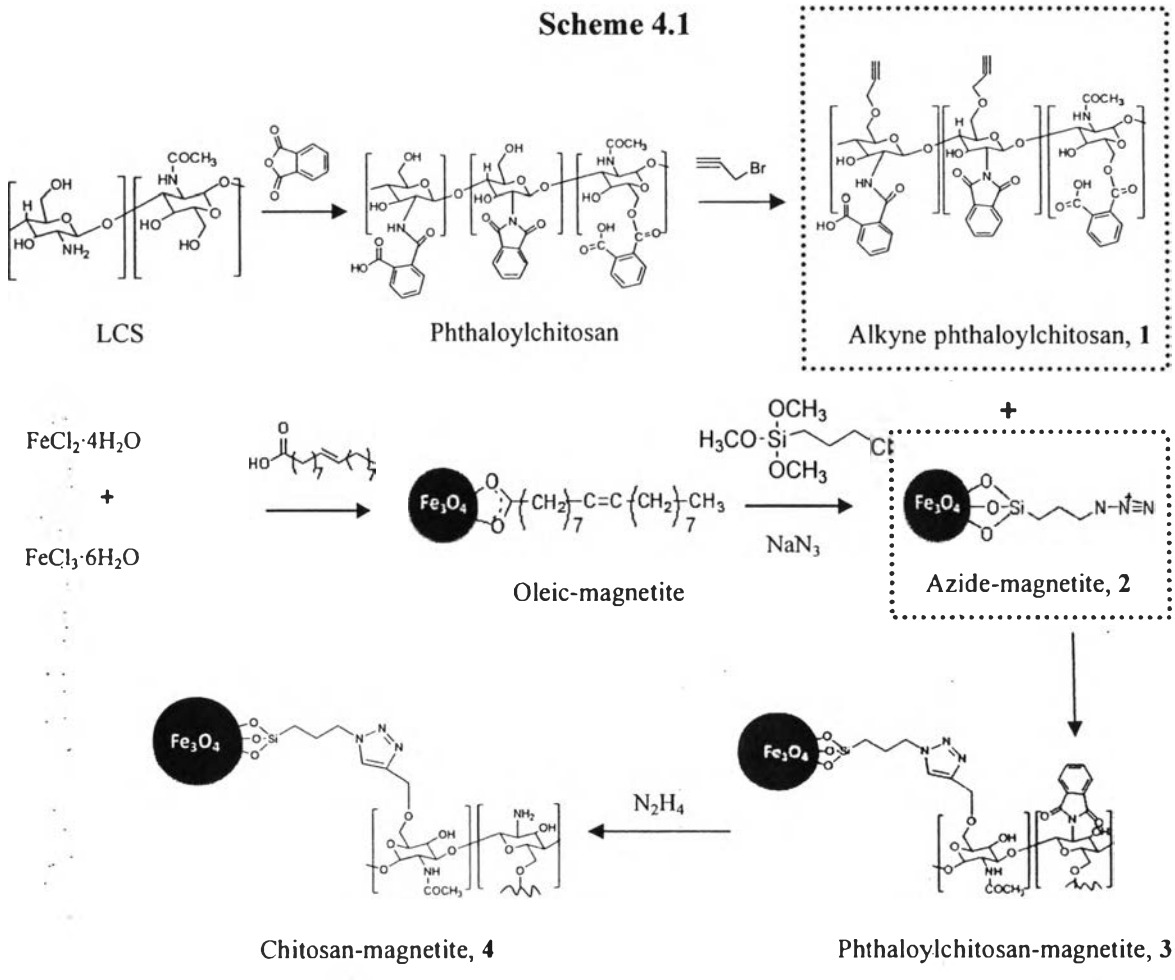

FTIR spectrum of **1** shows the characteristic peaks of C=O stretching of phthalamido at 1775 and 1714 cm^{-1}, and C-H deformation of *o*-disubstituted benzene at 794 cm^{-1} (Figure 4.1A) and C-C stretching of alkyne (C≡C) at 2129 cm^{-1} (Figure 4.1B).

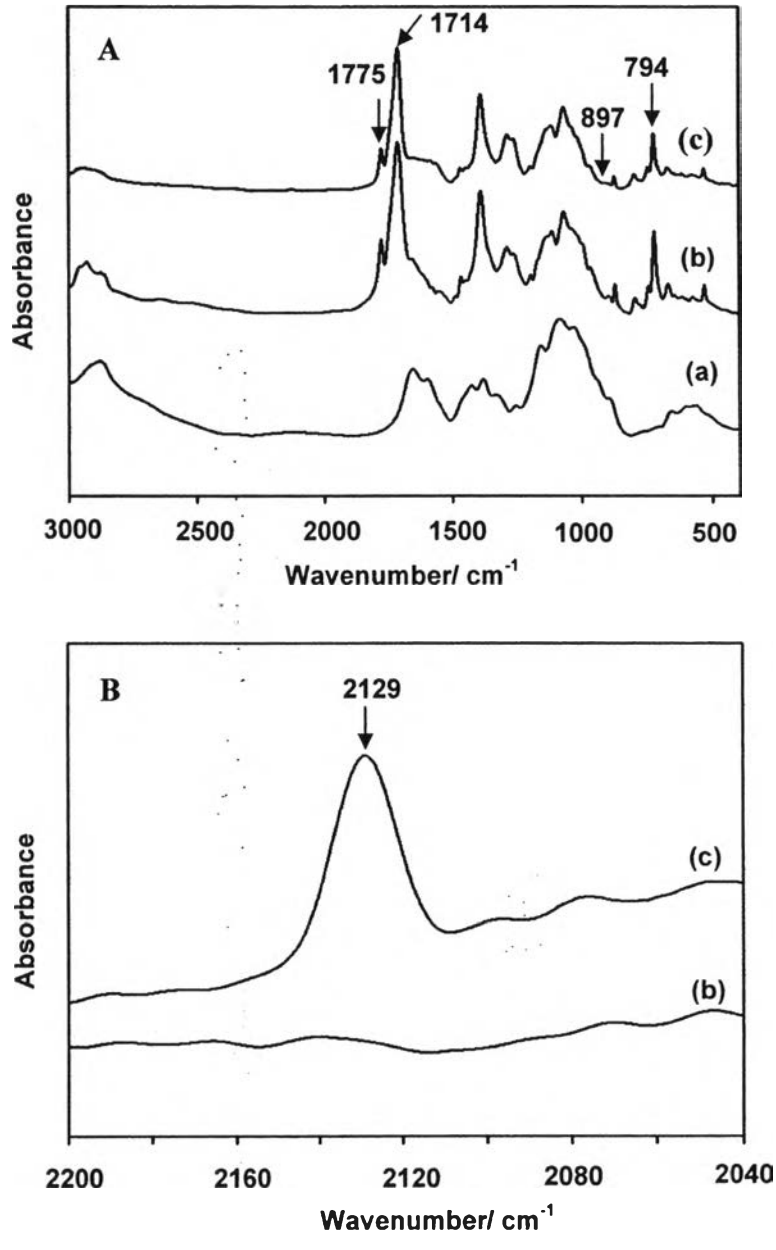

Figure 4.1 FTIR spectra of **A**; LCS (a), phthaloylchitosan (b), and alkyne phthaloylchitosan (c) in the range of 3000-400 $cm^{-1}$and **B**; phthaloylchitosan (b) and alkyne phthaloylchitosan (c) in the range of 2200-2040 cm^{-1}.

Alkyne phthaloylchitosan was obtained from the reaction of phthaloylchitosan and propargyl bromide in various types of base and temperatures for evaluating the optimum condition. The ratio of integration between C-C

stretching of alkyne at 2129 $cm^{-1}$and C-O-C stretching of pyranose at 898 cm^{-1} as an internal standard are considered as shown in Figure 4.2. The condition of KOH at 90°C shows the highest value of the integral ratio as compared to other temperatures and types of base. Therefore, this condition is an optimum to obtain alkyne phthaloylchitosan. Moreover, in the case of NaOH, the reaction did not give alkyne phthlaloylchitosan at any temperature because alkyne phthaloylchitosan precipitated in base (0.001M NaOH) during the reaction. Although NaH is a good base but it is easily oxidized with air, the use of this base is rather complicated. This step needs to be considered about the type of base and the reaction temperature, in other words, each base showed reactivity depending on the temperature.

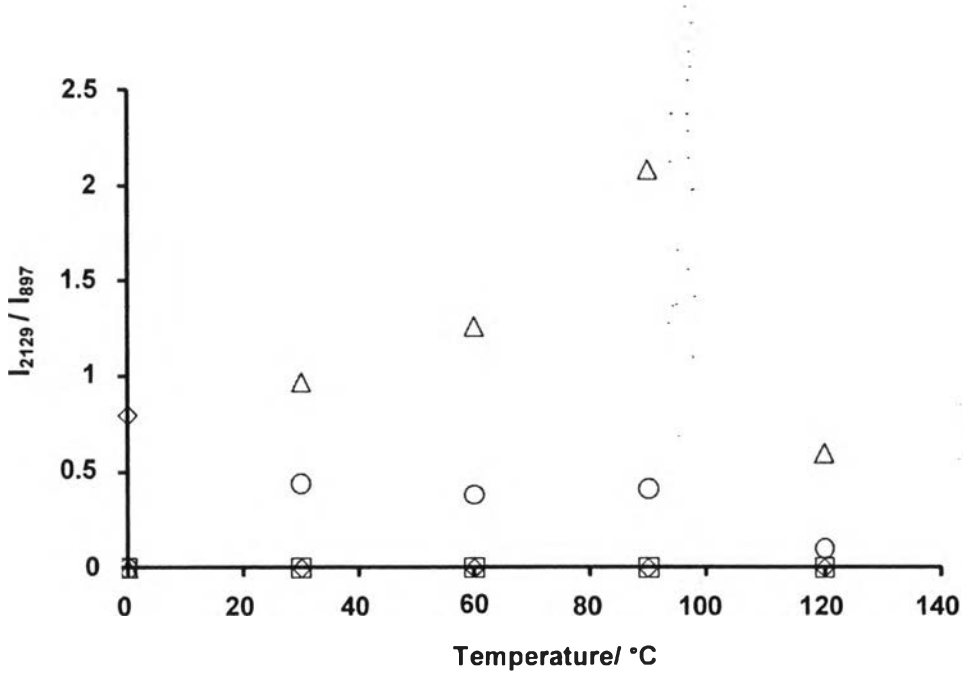

Figure 4.2 Temperature and I_{2129}/I_{897} ratio of alkyne phthaloylchitosan generating by incorporation of triethylamine (○), 0.001 M NaOH (□), KOH (Δ), and NaH (◇).

FTIR spectrum of **2** shows the characteristic peaks of -N=N=N- at 2039 cm^{-1}, Si-O at 1040 cm^{-1}, and Fe-O at 588 cm^{-1} as shown in Figure 4.3. In this step, polarity of solvent is a parameter to consider for an optimal condition of azide magnetite nanoparticles. The integral ratio of azide at 2098 cm^{-1} and internal standard belonging to Fe-O at 588 cm^{-1} were considered to determine the appropriate

solvent (Figure 4.4). The results suggest that DMF with polarity index 6.4 (Joseph, *et al.*, 1998) is an appropriate solvent to obtain azide magnetite nanoparticles because it shows the highest value of the integral ratio. Besides, the integral ratio of azide-magnetite nanoparticles with the incorporation of oleic acid is higher than no incorporation of oleic acid. This might be due to the different surface area of the particles. TEM micrograph (Figure 4.5) shows that the magnetite nanoparticles with oleic acid are individual particles whereas the magnetite particles without oleic acid are aggregated. Therefore, the magnetite nanoparticles with oleic acid can provide higher total surface area than magnetite nanoparticles without precoating with oleic acid.

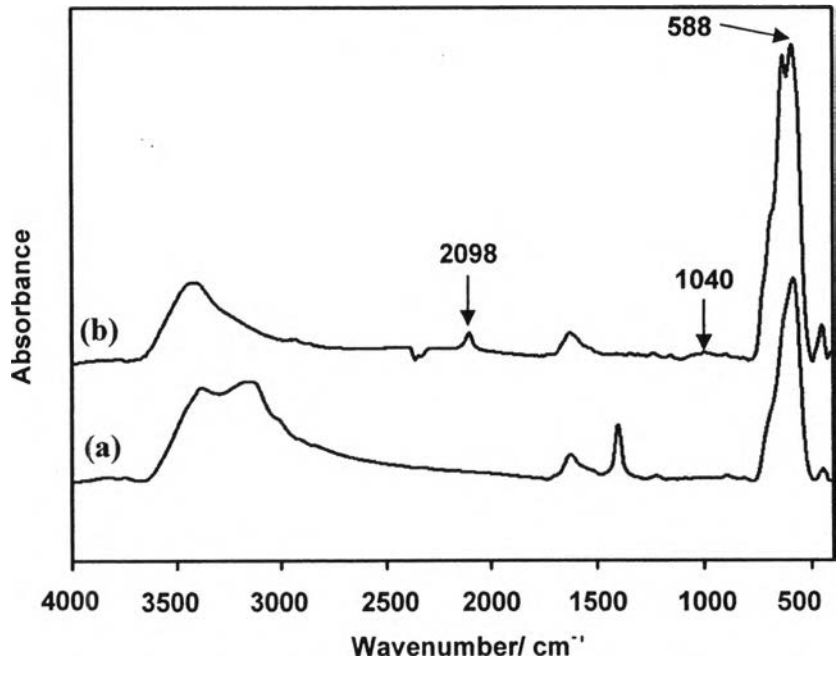

Figure 4.3 FTIR spectra of oleic-magnetite particles (a) and azide magnetite nanoparticles (b).

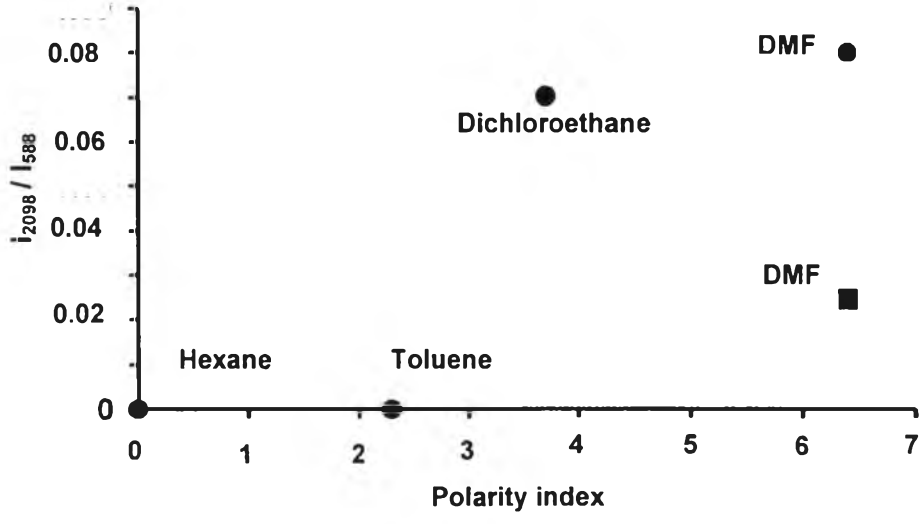

Figure 4.4 Polarity index of solvents and I_{2098}/I_{588} ratio of azide-magnetite nanoparticles by incorporating with oleic acid (●) and no oleic acid (■).

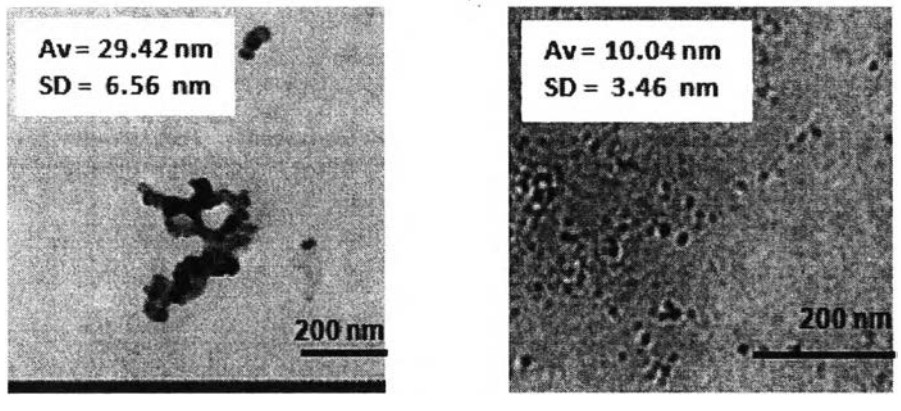

Figure 4.5 TEM micrographs of magnetite particles without oleic acid (a) and magnetite nanoparticles with oleic acid (b).

Compound **3** was obtained from the reaction of alkyne phthaloylchitosan and azide magnetite. FTIR spectrum of **3** shows a decrease of azide peak at 2098 cm^{-1} (Figure 4.6 (b)), this means that the azide functional group is changed to triazole bond. In this step, the temperature is a parameter to be carefully considered for the efficiency of the "click" reaction as there is no use of Cu(I) as a catalyst as found in general "click" chemistry. Figure 4.7 shows the optimal

temperature to be at room temperature as evaluated from the highest relative percent of triazole. The successful reaction can also be confirmed by TGA based on the amount of chitosan on the particles as shown in Figure 4.8. It should be noted that chitosan-magnetite nanoparticles via "click" chemistry show lower amount of chitosan content than non "click" one. This might be due to triazole groups of "click" reaction were occurred at specific positions between alkyne of chitosan and azide of magnetite nanoparticles. Chitosan-magnetite nanoparticles via "click" reaction shows the pyrolysis temperature at 460°C and this peak can not be seen in the case of the non "click" reaction (Figure 4.9). This implies "click" provides the stability of the triazole bond.

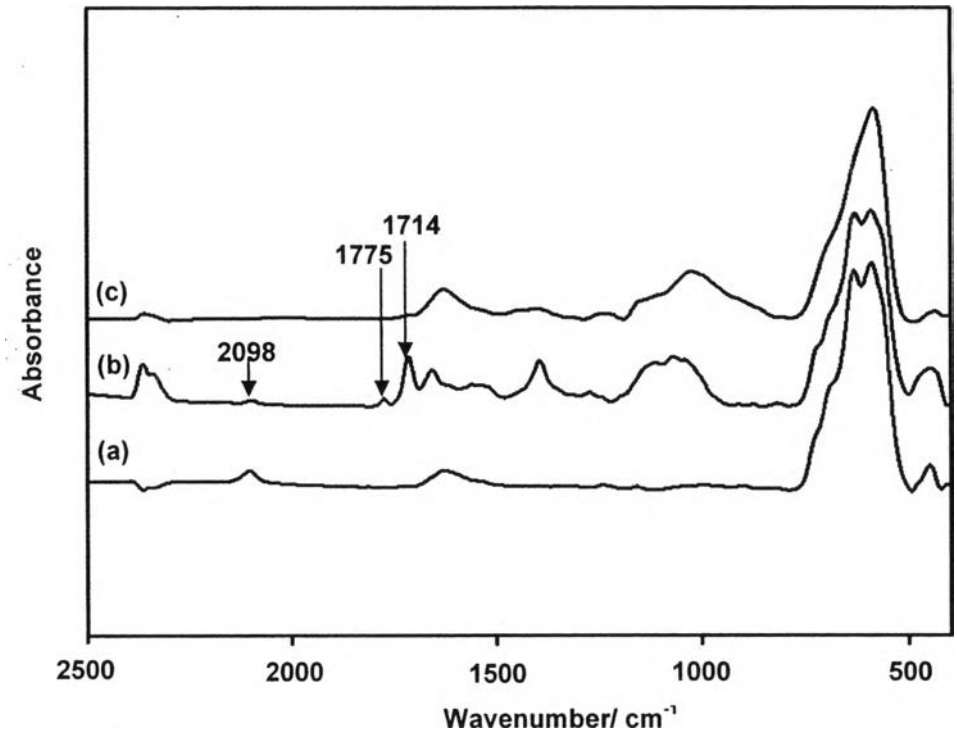

Figure 4.6 FTIR spectra of azide magnetite nanoparticles (a), phthaloylchitosan magnetite nanoparitcles (b), and chitosan magnetite nanoparticles (c).

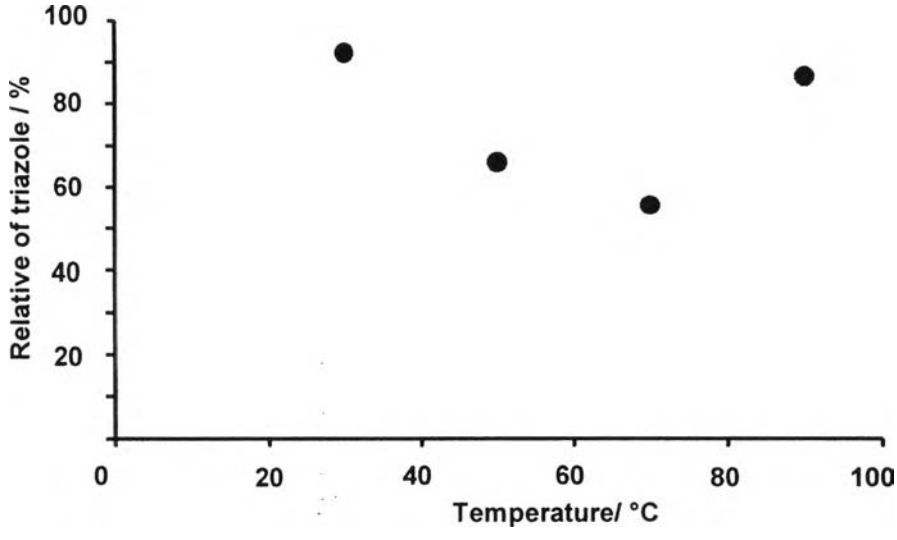

Figure 4.7 Temperature and percent of relative of triazole from FTIR data of the synthesis of chitosan-magnetite nanoparticles via "click" chemistry.

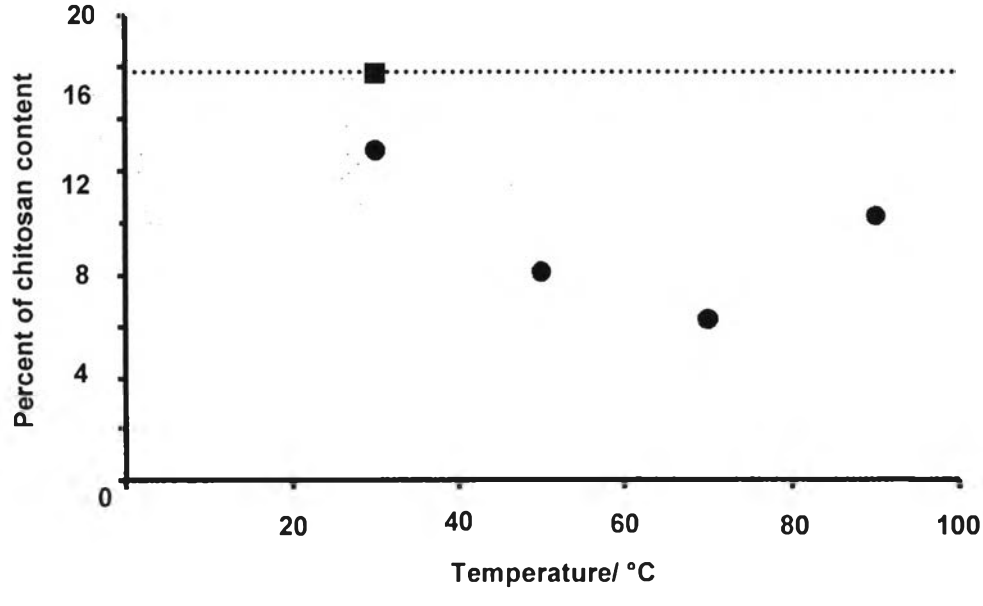

Figure 4.8 Temperatue and percent of chitosan content of synthesis of chitosan-magnetite nanoparticles via "click" chemistry (●) and chitosan-magnetite magnetite nanoparticles via non "click" chemistry (■).

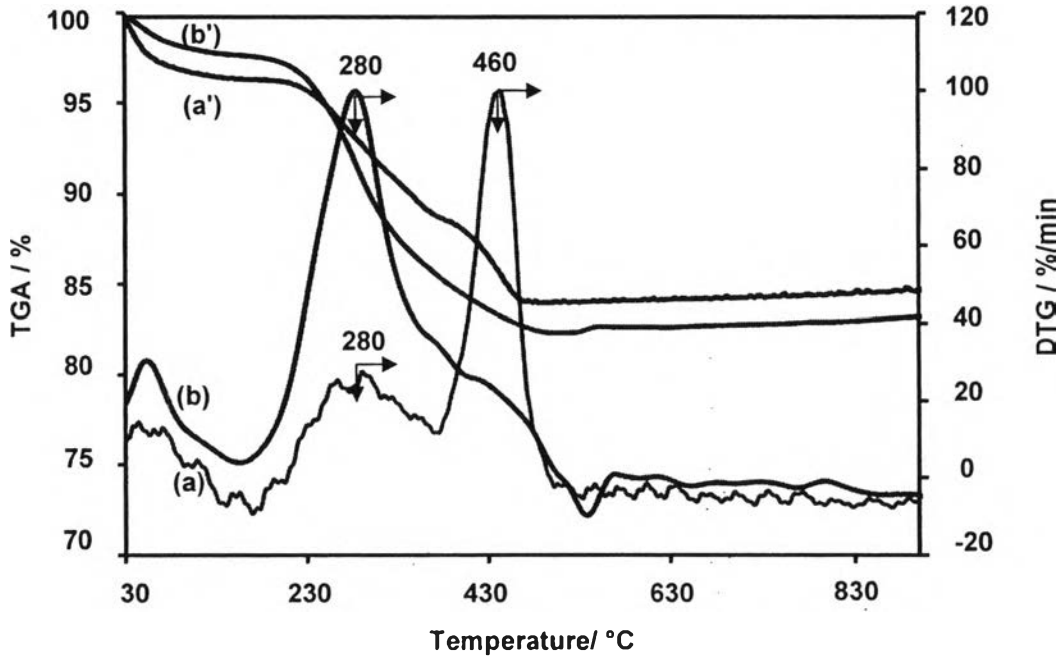

Figure 4.9 TGA thermograms of chitosan-magnetite nanoparticles via "click" chemistry (a) and chitosan-magnetite nanoparticles via non "click" chemistry (b) and DTG thermograms of chitosan-magnetite nanoparicles via "click" chemistry (a') and chitosan-magnetite nanoparticles via non "click" chemistry (b').

4.4.2 Confirmation of Iron Oxide Phase and Magnetic Property

Phase of iron oxide particles can be determined by using XRD. The XRD patterns (Figure 4.10) of azide-magnetite nanoparticles and chitosan-magnetite nanoparticles show the six characteristic peaks of magnetite phase at (220), (311), (400), (422), (511), and (440) whereas alkyne phthaloylchitosan shows the broad peaks regarding to amorphous phase. The magnetite nanoparticles coating with chitosan does not affect to change the phase of the magnetite nanoparticles.

The magnetic property of the magnetite nanoparticles evaluated by VSM is shown in Figure 4.11. The spectrum shows the superparamagnetic pattern, and magnetization of the particles is 63.361emu/g and coercivity is 24.497 G whereas magnetization of uncoated magnetite nanoparticles is 66.373emu/g and coercivity is 52.813 G. The higher superparamagnetic property is, the lower coercivity will be, this is because magnetic moment requires less energy to spin back

to the origin state, it means that, the particles respond to an applied external magnetic field and do not response to any unapplied external magnetic field, immediately.

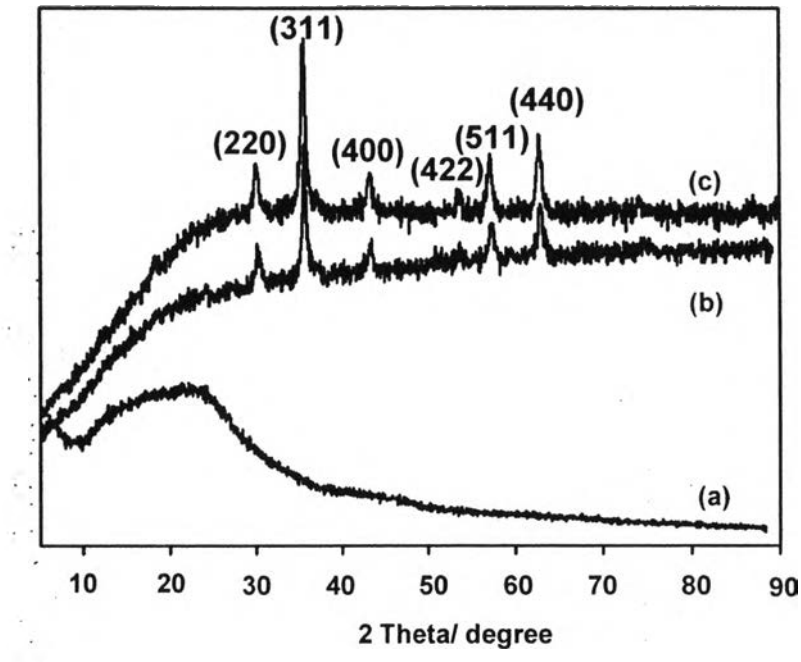

Figure 4.10 XRD patterns of azide phthaloylchitosan (a), azide magnetite nanoparticles (b), and chitosan magnetite nanoparticles (c).

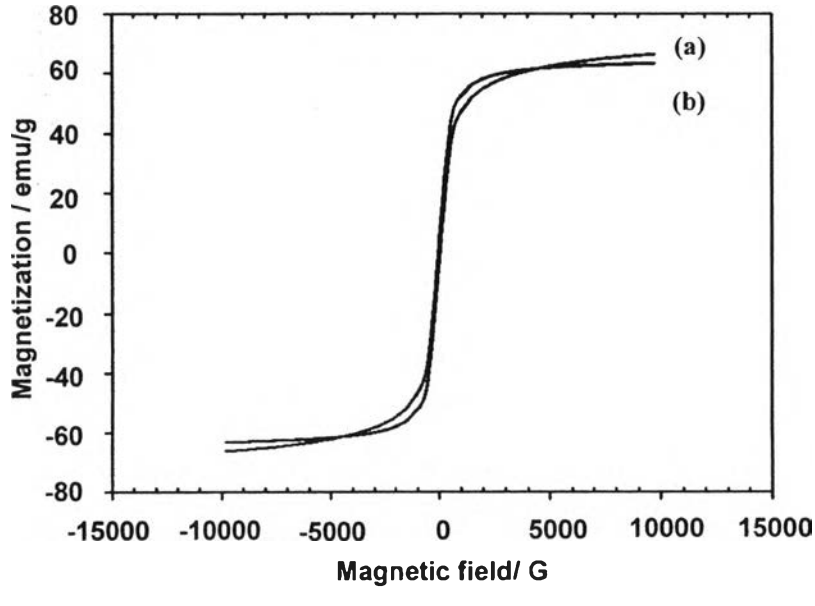

Figure 4.11 Hysteresis loop of uncoated magnetite particles (a) and chitosan-magnetite nanoparticles (b).

4.4.3 Effects of Solvent Polarity to Hydrodynamic Radius of the Particles

Chitosan-magnetite nanoparticles might show different behavior in different solvents based on polarity index. In the case of the nanoparticles in bad solvents (low polarity), the polymer chains tend to collapse whereas the nanoparticles in good solvents (high polarity), the polymer chains expanded as shown in Scheme 4.2. The hydrodynamic radius, R_h of the nanoparticles obtaining from DLS shows that the nanoparticle size in non-polar solvent which is hexane has the smallest size. The hydrodynamic radius of the nanoparticles tends to increase when the polarity index of the solvents increases as shown in Figure 4.12.

The nanoparticles show different dispersibility in various solvents as shown in Figure 4.13. This reflects how the polymer chain collapsed resulting in aggregation in bad solvent e.g. and expanded resulting in colloidal state in good solvents e.g.DMF and water.

Scheme 4.2

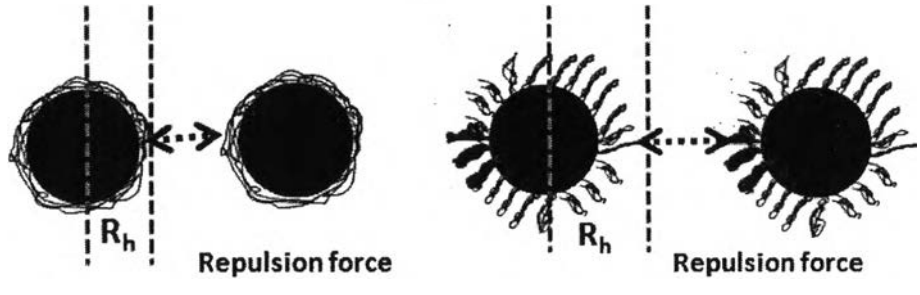

in bad solvent in good solvent

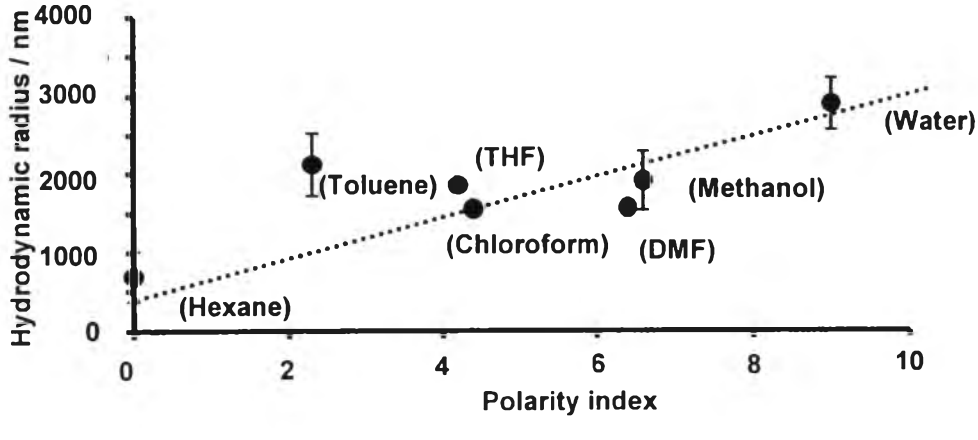

Figure 4.12 Polarity index and hydrodynamic radius of the chitosan-magnetite nanoparticles.

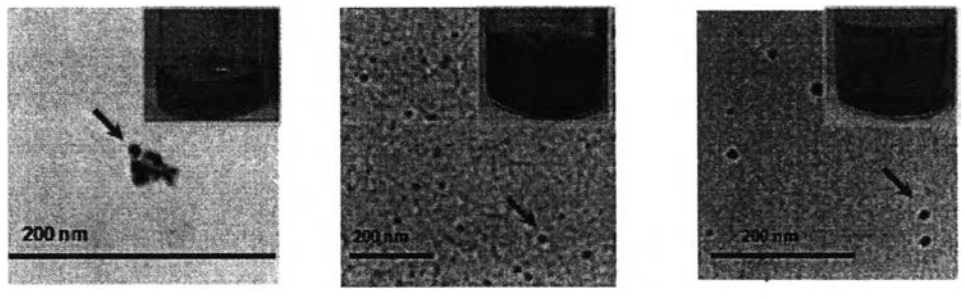

Average diameter=4.35 nm Average diameter=11.75 nm Average diameter=26.67 nm

(a) **(b)** **(c)**

Figure 4.13 TEM micrographs of the chitosan-magnetite nanoparticles in (a) hexane, (b) DMF, and (c) water.

4.4.4 Effect of pH on Hydrodynamic Radius of Chitosan-magnetite Nanoparticles

The buffer solutions with different pHs might possibly affects on hydrodynamic radius (R_h) of the chitosan-magnetite nanoparticles since the solution contains cationic and anionic species. Scheme 4.3 illustrates different performances of chitosan-magnetite nanoparticles in different pHs. At pH 2-3, the effect of positive charges is significant whereas at pH 11-12, the effect of negative charges becomes the main. The fact that the size of the negative charges is bigger than the positive charges therefore the negative charges provide a higher expansion of the polymer chains than the positive charges. The nanoparticles show different R_h in different pHs as shown in Figure 4.14. The average R_h of the nanoparticles at pH 4-10 is lower than those at pH 2-3 and at pH 11-12. This might be due to the amount of cations and anions in buffer solution tend to balance the charge on polymer chain at this pH condition. TEM micrographs (Figure 4.15) also show the biggest size of nanoparticles at pH 11.

Scheme 4.3.

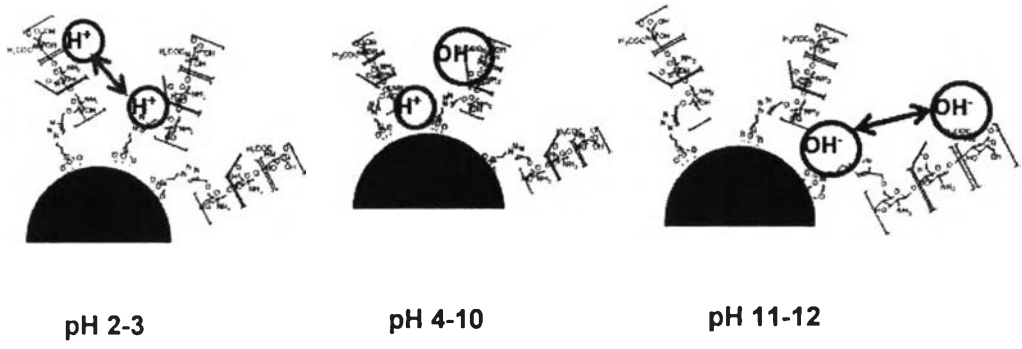

pH 2-3 pH 4-10 pH 11-12

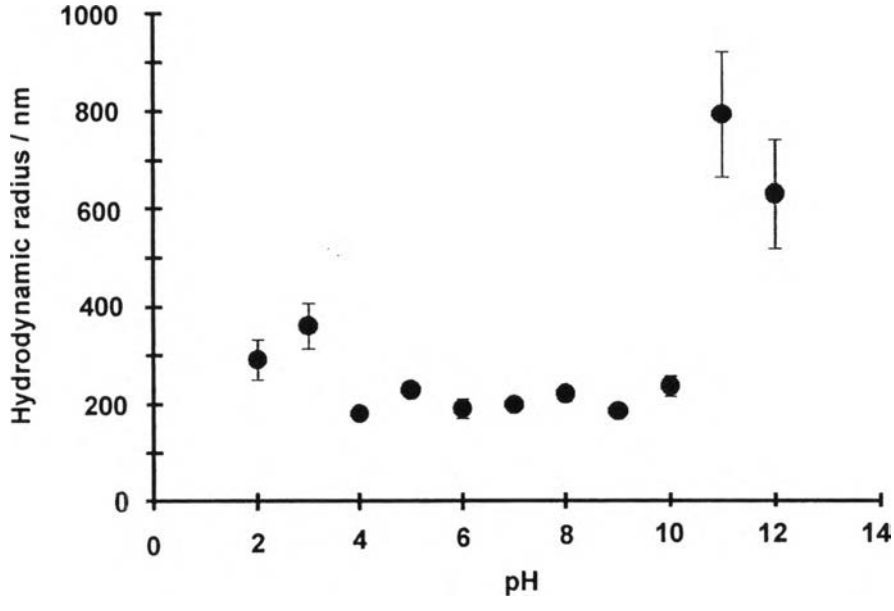

Figure 4.14 PBS buffer solution with different pH and hydrodynamic radius of the chitosan-magnetite nanoparticles.

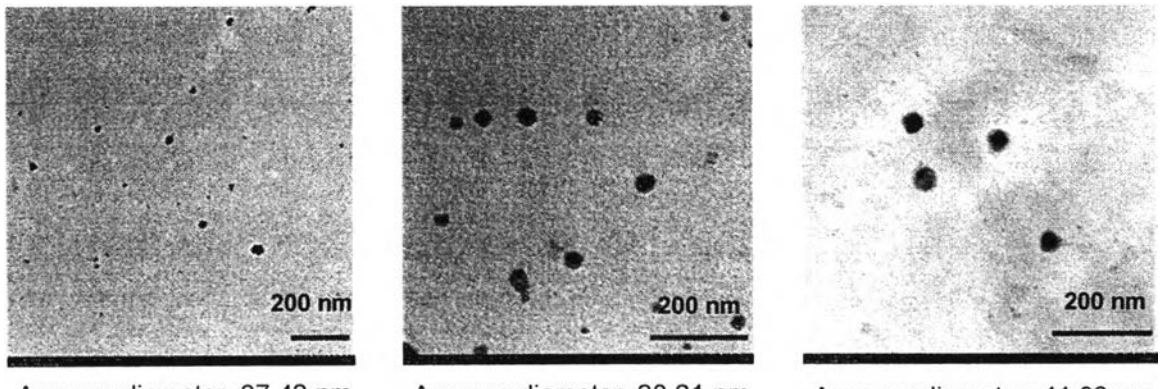

Average diameter=27.42 nm (a)

Average diameter=28.21 nm (b)

Average diameter=41.92 nm (c)

Figure 4.15 TEM micrographs of the chitosan-magnetite nanoparticles in (a) pH 3, (b) pH 6, and (c) pH 11 under different PBS buffer solutions.

4.4.5 Effect of pH on Surface Charge of the Chitosan-magnetite Nanoparticles

The condition of different pH has effect to zeta potential of the chitosan-magnetite nanoparticles as shown in Figure 4.16. The zeta potential reflects the stability of the particles as summarized in Table 4.1. Figure 4.16 shows that at pH 2, the zeta potential of chitosan-magnetite nanoparticles is about -20 mV implying the incipient instability whereas at pH 3, the value is about -55 mV referringto good stability. The pH range between 4 and 13, shows the zeta potential about -60 to -100 mV referring to the nanoparticles with excellent stability. This high (more than ±60 mV) zeta potential provides the higher repulsive force between charges on the surface of the particles resulting in the colloidal stability.

Table 4.1. The zeta potential with stability behavior of the colloidal solutions

Zeta potential (mV)	Stability behavior of the colloidal solution
from ±10 to ± 30	Incipient instability
from ±30 to ± 40	Moderate stability
from ±40 to ± 60	Good stability
more than ± 61	Excellent stability

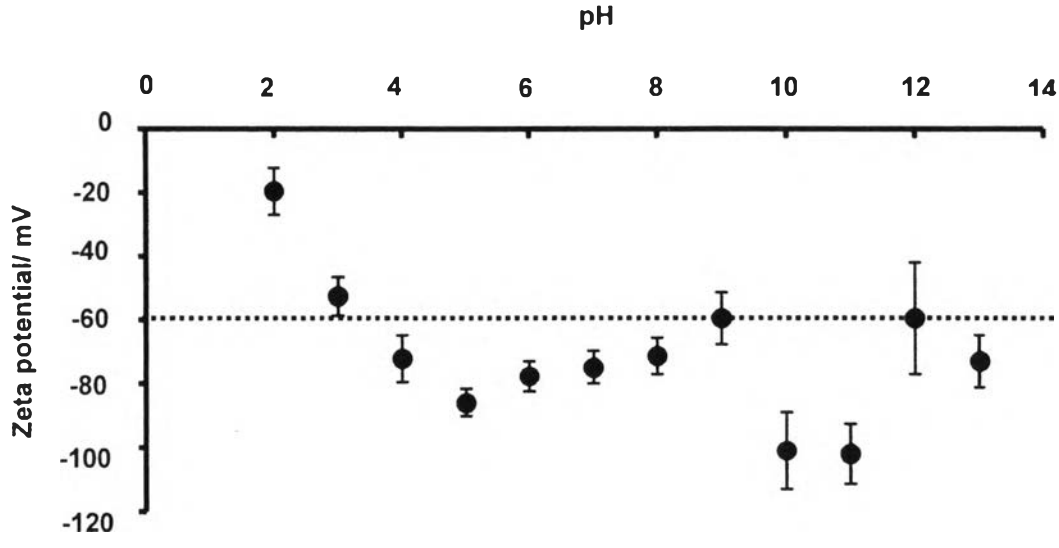

Figure 4.16 Zeta potential of chitosan-magnetite nanoparticles in different pHs of PBS buffer solution.

4.4.6 Preliminary Study of pDNA Separation

The results of the pDNA separation of the magnetite nanoparticles as shown in Table 4.2. Chitosan-magnetite nanoparticles via "click" chemistry shows lower pDNA trapping ability as compared to the commercial product namely, Dynabeads.® Comparing the pDNA trapping of chitosan-magnetite nanoparticles via "click" chemistry to that of chitosan-magnetite nanoparticles via non "click" chemistry, it is found that the percent trapping is similar. This implies the function of triazole in binding with pDNA might be as similar to that of amino group in chitosan.

Table 4.2. Percent of DNA trapping of Dynabeads®, chitosan-magnetite nanoarticles ("click" chemistry), chitosan-magnetite nanoparticles (non "click" chemistry)

Samples	A_{260}	DNA trapping (%)
DNA of *E.coli*	1.489±0.0018	-
Dynabeads®	0.698±0.0004	53.12
Chitosan-magnetite nanoparticles ("click" chemistry)	1.288±0.0018	13.50
Chitosan-magnetite nanoparticles (direct conjugation)	1.278±0.0008	14.17

4.5 Conclusions

Chitosan-magnetite nanoparticles were successfully synthesized via Cu(I) free "click" chemistry in mild condition to obtain triazole linkage providing hydrogen bond. The nanoparticles obtained are magnetite phase with superparamagnetic properties. They have good dispersion and high stability in PBS buffer solution at pH 4-13. Besides, the hydrodynamic radius and individual size of the particles have significance in different solvents polarity. The preliminary study of the chitosan-magnetite nanoparticles via "click" chemistry showed a good possibility to separate pDNA that might due to additional triazole linkage to have some specific interaction with the pDNA in media.

4.6 Acknowledgements

The author acknowledges the scholarship from the Development and Promotion of Science and Technology talents project (DPST) and fund from the National Center of Excellence for Petroleum, Petrochemicals, and Advanced Materials, Thailand. The author would like to extend their thankfulness to the Petroleum and Petrochemical College, Chulalongkorn University for academic knowledge and facilities. The author deeply thanks the National Nanotechnology Center (NANOTEC), The National Science and Technology Development Agency (NSTDA) of Thailand (Project No. : NN-B-2-FN1-10-52-14) for fund and the Hitachi-High Technology Co., Ltd., Japan for TEM analysis.

4.7 References

1. **Berry, C. and Curtis, A.S.G.** (2003). Appl. Phys. B, 36, R198-R206.
2. **Gupta, A.K. and Gupta, M.** (2005). Biomaterials 26, 3995-4021.
3. **Hildebrandt, B., Wust, P., Ahlers, O., Dieing, A., Sreenivasa, G., Kerner, T., Felix, R. and Riess, H.** (2002). Crit. Rev. Oncol. Hematol. 43, 33–56.
4. **Kawai, N., Futakuchi, M., Yoshida, T., Ito, A., Sato, S., Taku, N., Honda, H., Shirai, T. and Kohri, K.** (2008). Prostate 68, 784-792.

5. **Kim, E.H., Ahn, Y. and Lee, H.S.** (2007). J. Alloys compd, 43(4), 633-636.
6. **Kolb, H. C., Finn, M. G. and Sharpless, K. B.** (2001). Angew. Chem. Int. Ed. 40 (11), 2004–2021.
7. **Mincheva, R., Stoilova, O., Penchev, H., Ruskov, T., Spirov, I., Manolova, N. and Rashkov, I.** (2008). J. Eur. Polym. 44, 615-627.
8. **Nishimura, S., Kohgo, O., Kurita, K. and Kuzuhara, H.** (1991). Macromolecules 24(17), 4745-4748.
9. **Randy, D. P., Sara, P., Margriet, J., Van, B., Heidi, V., Den, R., Kristien, B., Wim, L., Jules, M., Gustaaf, B. and Guido, M.** (2007). Chem. Mater. 19, 1821-1831.
10. **Šafařík, I. and Šafaříková, M.** (2004). Biomagn. Res. Technol. 2, 7.
11. **Sun, J., Zhou, S., Hou, P., Yang, Y., Weng, J., Li, X. and Li, M.** (2006): J. Biomed. Mater. Res. DOI: 10.1002/jbm.a.30909.
12. **Wust, P., Hildebrandt, B., Sreenivasa, G., Rau, B., Gellermann, J., Riess, H., Felix, R. and Schlag P.M.** (2002). Lancet Oncol. 3, 487–497.
13. **Yoksan, R., Akashi, M., Hiwatari, K-I. and Chirachanchai, S.** (2003). Biopolymers 69(3), 386-390.
14. **Zampano, G., Bertoldo, M. and Gardeli, F.** (2010). React. Funct. Polym. 70, 272-281.
15. **Zhang, L., He, R. and Gu, H.** (2006). Appl. Surf. Sci. 253, 2611-2617.